SECOND EUROPEAN CONFERENCE ON EARTHQUAKE ENGINEERING
AND SEISMOLOGY, ISTANBUL AUG. 25-29, 2014

BLIND PREDICTION TESTS AS A BENCHMARK TO IMPROVE THE SEISMIC RESPONSE OF FIBRE MODELS

Romain SOUSA[1], António A. CORREIA[2], João P. ALMEIDA[3] and Rui PINHO[4]

ABSTRACT

The seismic behaviour of reinforced concrete framed structures involves a number of nonlinear material and geometrical phenomena that are impossible to model exhaustively in a single model. Furthermore, past studies showed that the most correct modelling options from the scientific viewpoint are sometimes challenged by experimental results. Over the years, attempts have been made to identify and measure the importance of different modelling options. This work intends to consolidate some of these findings and further extend them in order to progressively bridge the gap between solidly established theoretical principles and shaking table test results. The response of three different structures used in international blind prediction test challenges serves as benchmark to assess the goodness-of-fit of alternative numerical solutions. The interpretation of the results highlights the sensitivity of the response with respect to the modelling choices and provides indications towards the development of optimized numerical analyses.

INTRODUCTION

Primarily impelled by the exponential growth of computational capabilities and supported on numerous experimental observations and advanced algorithms, structural engineers have now several software packages available which are capable of performing advanced seismic analysis of complex structures. Furthermore, seismic design and assessment of structures is becoming increasingly dependent on numerical simulation tools.

Past blind prediction contests showed that, by using appropriate modelling options, the seismic response of structures could be predicted with appreciable accuracy. Nonetheless, the global comparison of the competitors' predictions reveals a large dispersion of the submitted results, even when computed with the same structural analysis package. This observation points towards the need to identify the main sources of inaccuracy in nonlinear analysis and to clarify which seem to be the best modelling criteria in order to minimize the gap between experimental and numerical response parameters. Fig.1, which shows the results obtained in a past blind prediction contest (NEES@UCSD, 2010), demonstrates the ability to produce accurate predictions for different response parameters. However, the large dispersion clearly exposes the current difficulties in selecting the most appropriate modelling options despite the simplicity of the tested specimen.

[1] Ph.D. Student, ROSE Programme, UME School, IUSS Pavia, Pavia, romain.sousa@umeschool.it
[2] Postdoctoral Researcher, National Laboratory for Civil Engineering, Lisbon, aacorreia@lnec.pt
[3] Postdoctoral Researcher, École Polytechnique Fédérale de Lausanne, Lausanne, joao.almeida@epfl.ch
[4] Asst. Prof., Dept. of Civil Engineering and Architecture, University of Pavia, Pavia, rui.pinho@unipv.it

Figure 1. Comparison between experimental response and numerical predictions from the "Concrete Column Blind Prediction Contest 2010" (adapted from NEES@UCSD (2010))

Over the last years, attempts have been made to identify and measure the importance of different modelling options (e.g., Sousa et al. (2012) and Yazgan and Dazio (2011a, 2011b)). The current work intends to consolidate some of these findings and further extend them in order to progressively bridge the gap between solidly established theoretical principles and shaking table test results. In particular, following some theoretical considerations, a sensitivity study is carried out on the following parameters:

- Equivalent viscous damping (EVD)
- Element formulation and discretization scheme
- Strain penetration (SP) and anchorage slip

The response of three different structures subjected to shaking table tests will serve as a benchmark for comparison purposes. The goodness-of-fit of each approach, assessed in terms of lateral displacements and accelerations, is determined based on the error associated with the peak values measured during each time-history record, together with a frequency-domain approach capable to evaluate the records under comparison in terms of both amplitude and frequency content.

THEORETICAL CONSIDERATIONS

This section recalls, in a succinct manner, the relevant theoretical background relative to the modelling options considered in the current sensitivity study.

Damping

Damping in structures is generally associated with the decay of free-vibration motion due to energy dissipation mechanisms in both structural and non-structural components. In real structures, several irreversible thermodynamic processes concur to such decay, e.g., global damage in the components, internal friction between the materials or at connections, opening and closing of micro-cracks in the materials, and friction between the structure itself and non-structural elements (Chopra, 1995).

Within the scope of nonlinear frame analysis, the majority of dissipated energy is accounted for explicitly through material hysteresis. The use of generalized damping is however needed to reproduce sources of energy dissipation that, given their phenomenological complexity, are difficult to explicitly model. Hence, the required damping for a given nonlinear dynamic analysis will necessarily depend on the level of detail of the model and the capabilities of the numerical tool used. Given the difficulties to identify and mathematically describe each of these dissipating mechanisms in actual structures, damping is usually represented in a highly idealized manner by a set of generalized linear viscous dampers. The damping coefficients are selected so that the dissipated energy is equivalent to the energy associated to all un-modelled dissipation mechanisms. This idealisation is therefore called *equivalent* viscous damping (EVD).

The most conventional EVD approach assumes that the damping forces developed in structures are proportional to the structural initial (elastic) stiffness, regardless of the level of ductility developed. Considering the stiffness degradation resulting from structural damage, this solution may result in an overestimation of the energy dissipated through viscous damping. Analysis performed by Priestley and Grant (2005) indicate that in this case, the energy absorbed by elastic damping may approximate the energy dissipated through hysteresis, even for high ductility levels. Consequently, it is not surprising

that such damping model could produce a significant underestimation of peak response displacements. Moreover, as the stiffness decreases, the damping forces may assume unrealistically large values when compared to the member (restoring) forces (Hall, 2006). Additionally, Bernal (1994) showed that spurious damping forces are likely to arise at the presence of massless DOFs, or with relatively small inertia. Under such conditions, massless DOFs have the tendency to undergo abrupt changes in velocity when stiffness changes, leading to unrealistically large viscous damping forces (Jehel et al., 2013). Finally, the use of stiffness-proportional damping (SPD) may artificially introduce significant axial forces at the members, leading to convergence issues and potentially unstable analyses.

The use of tangent stiffness-proportional damping (TSPD), on the other hand, seems to be the most consensual option within the scientific community. It represents a decrease in the energy dissipated through EVD for increasing ductility demands, which reflects an intuitively acceptable physical concept. Nevertheless, this model presents also significant setbacks, namely because when the stiffness matrix becomes negative definite (i.e., softening response), this leads to an unrealistic input of energy in the structure. Moreover, as demonstrated by Correia et al. (2013), when using (initial or tangent) stiffness-proportional damping, the forces at the members are not in equilibrium with the support reactions.

Despite not having an easily identifiable physical meaning, the mass-proportional damping (MPD) approach does not exhibit the numerical deficiencies of the previous models. Nonetheless, Hall (2006) reported several weaknesses when large rigid body modes occur in the structures, leading to excessively high velocities. This situation is not common in traditional structural engineering problems but may be important when dealing with base-isolated structures. In addition, the damping ratio in MPD models decreases exponentially with a decrease of the period of vibration, thus possibly leading to an underdamped higher-mode response.

In the present study, four different EVD models are considered: no damping, initial stiffness-proportional damping (ISPD), tangent stiffness-proportional damping (TSPD), and mass-proportional damping (MPD). Additionally, increasing percentages of critical damping, ranging from 0.5% to 5%, were assigned to the fundamental period of vibration.

Element Discretization

A first and crucial decision—often conditioned by the available structural software package—that every engineer faces when modelling a frame structure for seismic analysis, is related to the choice of the element model. Lumped plasticity approaches are simpler and computationally lighter, but they do not allow modelling the spread of inelasticity throughout the member. In addition, the use of such approach requires an *a priori* knowledge of the location and extent where the inelasticity will concentrate—something that, according to recent studies, e.g., Hines et al. (2004), may vary significantly depending on the level of ductility demand. Moreover, modelling elements through lumped plasticity models requires a high level of expertise in order to define the appropriate moment-curvature diagram at the critical section taking into account the material degradation and variations in the axial force.

Alternatively, the so-called distributed plasticity models allow modelling the spread of inelasticity along the member. FB and DB formulations are available, which verify equilibrium along the element length in an exact and average way, respectively. In view of this clear advantage of the FB approach, it was adopted in the numerical models used.

If or while the sectional behaviour does not surpass an eventual peak in the moment-curvature relation, the pernicious effects of numerical localization do not occur and the response is objective; hence, an adequate reproduction of the spread of inelasticity along the structural member only requires a sufficient number of integration points (IPs) per element, in order to attain a satisfactory numerical accuracy. On the other hand, if there is a sectional post-peak response, the objectivity of the results can only be guaranteed if regularization techniques are employed; several recent proposals can be found for FB elements, either based on fixed integration methods (Coleman and Spacone (2001); Scott and Fenves (2006) and Scott and Hamutçuoğlu (2008)) or adaptive commutation between schemes (Almeida et al., 2012).

Different numbers of IPs were considered to evaluate the effect of distinct discretizations on the global response of the structures. Hence, the number of IPs in each element was defined such that the weighted length of the IPs at the extremities of the members corresponds to either the total expected

plastic hinge length (L_P) or to one-half of that value, determined using the expressions proposed by Priestley et al. (2007):

$$L_P = kL_C + L_{SP} \geq 2L_{SP} \quad (1)$$

where

$$k = 0.2\left(\frac{f_u}{f_y} - 1\right) \leq 0.08 \quad (2)$$

accounts for the steel hardening properties, L_C is the shear span of the element, f_y and f_u are the yielding and ultimate strength of the longitudinal rebars, and L_{sp} is the strain penetration length determined by Eq.(3). In addition, a model featuring 10 IPs, representative of a highly discretized element is also considered. Following the recommendations proposed by Calabrese et al. (2010), the reference model is taken as the one featuring a number of IPs such that the weighted length of the IPs at the member ends approximates the expected plastic hinge length. It should be noted that, although a well-known formula for the plastic hinge length was used, it corresponds to an *equivalent* length for lumped plasticity analysis and not to the *true* plastic hinge length (as it should). Table.1 summarises the number of IPs considered for the columns of each structure. The number of elements used to model the beams of Structure 2 and Structure 3 vary depending on the reinforcement details along the members. Due to space limitations and the fact that beam modelling did not greatly affect the results, no further details are herein provided.

Strain Penetration

Reinforced concrete (RC) members subjected to flexure tend to suffer from localized deformations occurring at the connection between adjacent members (beam-column and /or column-footing joints). According to Sritharan et al. (2000) and Sezen and Moehle (2004), the total lateral displacement of RC members can increase by up to 40% due to bar slippage. Despite the relative importance of considering strain-penetration deformations, bond slip is often neglected in most numerical analysis of RC structures.

Numerous authors have proposed alternative ways to determine and numerically accommodate strain-penetration effects. The development of 3D solid finite element models to explicitly model the interaction between the longitudinal rebars and the surrounding concrete (e.g., Salem and Maekawa (2004) and Jendele and Cervenka (2006)) seems to be the most representative way to describe such behaviour. Alternatively, in the scope of beam formulations, Monti and Spacone (2000) and Girard and Bastien (2002) presented finite elements that explicitly account for the slip between the reinforcing bars and the surrounding concrete in the state determination at the section level. Although less time demanding than solid finite elements, the latter models are still computationally expensive given the extensive discretization required to accurately capture the actual rebars' response (Zhao and Sritharan, 2007). Based on the above-mentioned limitations, the use of a joint element appears as a natural alternative solution. The core philosophy of these models is based on the assumption that the strain-penetration deformations developed at a given member can be lumped into a single element located at the corresponding end (usually in the form of a zero-length element). The properties of the joint elements are generally derived based on empirical data and can be defined at the material level (reinforcement and concrete; e.g., Zhao and Sritharan (2007)) or at the sectional level with suitable moment-rotation relationships (e.g., Sezen and Moehle (2004)). Despite the associated simplicity, such models are not implemented in most current software packages, thus precluding its generalized use by structural engineers.

A simpler approach involves the extension of the element length by an estimated strain-penetration length. This approach relies on the assumption that the nonlinear response of the member spreads into the anchorage zone along the strain-penetration length, and consequently contributes to the overall member deformation.

Table 1. Element discretization scheme adopted for the different structures

	End IPs = L_P	End IPs = 0.5 L_P	10IPs
Structure 1	6 IPs: 2 elem. (3 + 3)	7 IPs: 2 elem. (4 + 3)	1 elem. (10 IPs)
Structure 2	1 elem. (4 IPs)	1 elem. (6 IPs)	1 elem. (10 IPs)
Structure 3	1 elem. (4 IPs)	1 elem. (6 IPs)	1 elem. (10 IPs)

According to Priestley et al. (2007), the strain-penetration length depends on the yield stress and diameter of the longitudinal reinforcement:

$$L_{SP} = 0.022 f_{ye} d_{bl} \ \ (f_{ye} \ in \ MPa) \tag{3}$$

where f_{ye} is the expected yield stress and d_{bl} is the diameter of the longitudinal rebars. This option seems to be particularly suitable to predict the response of structures that are expected to respond in the nonlinear range. Nonetheless, a significant setback relies on the fact that the additional deformation is achieved at the expense of considering a globally more flexible element (even when responding elastically) instead of a progressive additional rigid body rotation at the end(s) of the element. Moreover, considering that the shear span of the element increases for the same flexural capacity, the shear forces computed with a longer element will necessarily be underestimated.

An alternative option is to consider a rotational spring at the base of the columns, keeping the element dimensions unchanged. The elastic stiffness of this spring is determined such that the element develops the same lateral yield displacement than an identical element, fixed at the base, elongated by the strain-penetration length. A graphical interpretation of the latter approaches is presented in Fig.2. Following the reasoning behind the following figure, one can estimate the rotational stiffness (K_θ) at the base of the element through Eq.(4) (Correia, 2011).

In order to evaluate the importance of strain-penetration effects, three different solutions were considered in the numerical models: (1) base spring with constant rotational stiffness, (2) elongated element, and (3) strain penetration neglected. In the first approach, the rotational stiffness considered to reflect the additional flexibility resulting from the strain penetration of the longitudinal rebars was determined with Equation (4), and resulted in the following values: $K_\theta = 2610 \text{x} 10^3$ kNm/rad, $K_\theta = 7000$ kNm/rad and $K_\theta = 7450$ kNm/rad for Structure 1, 2 and 3, respectively.

For the elongated element approach, the strain-penetration length was determined based on Equation (1). The values obtained were: $L_{sp} = 0.41$ m for Structure 1 and $L_{sp} = 0.12$ m for Structures 2 and 3.

SENSITIVITY ANALYSIS

Case Studies

To carry out the sensitivity analysis, the results of three structures used in international blind prediction test challenges were selected as benchmarks. The first structure under analysis is a full-scale RC bridge column used in the "Concrete Column Blind Prediction Contest 2010", sponsored by PEER and NEES (NEES@UCSD, 2010). The specimen was tested under six consecutive ground motions of varying intensity. The 1.2 m diameter cantilevered column spans 7.2 m from the footing, as shown in Fig.3 (left). A massive 230 tonne reinforced concrete block supported by the column simulates the superstructure weight.

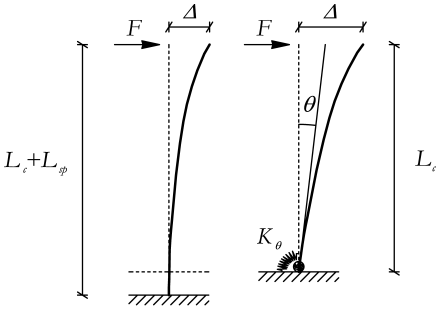

$$K_\theta = 3EI_y \frac{L_c^2}{\left[(L_c+L_{sp})^3 - L_c^3\right]} = \frac{M_N}{\phi_y} \frac{3L_c^2}{\left[(L_c+L_{sp})^3 - L_c^3\right]} \tag{4}$$

Figure 2. Graphical representation of longer element and base spring approaches (left) and associated rotational stiffness equation (Correia, 2011)

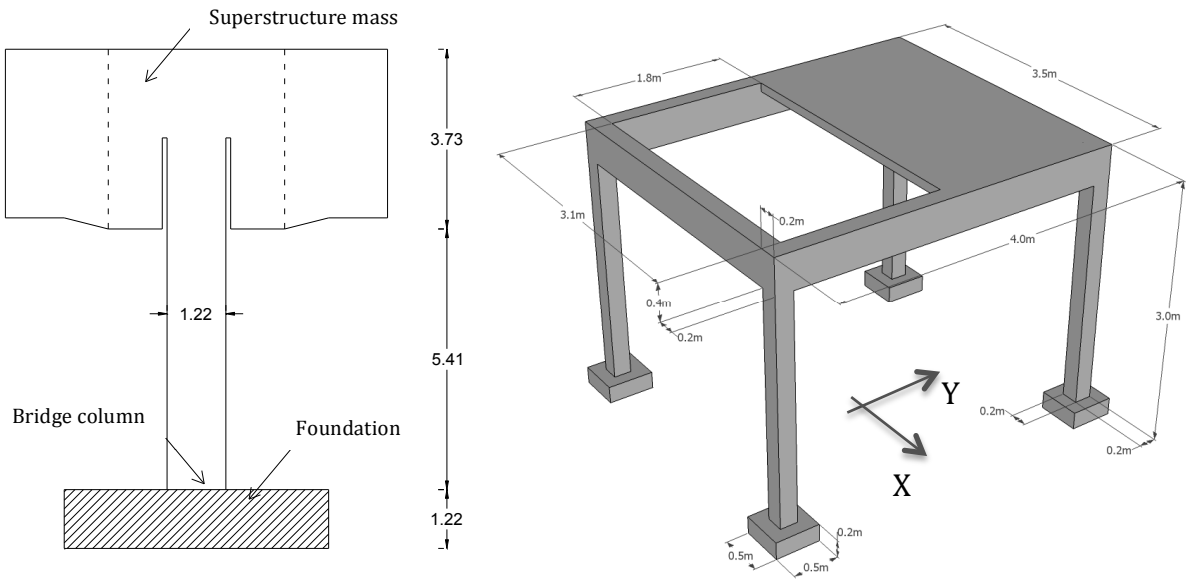

Figure 3. General dimensions of structure 1 (left) and Structure 2 and 3 (right)

Normal-weight concrete was used for the construction of the column, with a cylinder compressive strength of 42 MPa. The reinforcement of the column consisted of 18∅36 mm as longitudinal reinforcement (longitudinal volumetric ratio equal to 1.57%) and butt-welded ∅16 mm double hoops, spaced at 152 mm on-centre, as transverse reinforcement (transverse volumetric ratio equal to 0.96%). The yield and ultimate strength of longitudinal steel was 519 MPa and 707 MPa, whilst for the transversal reinforcement those values are 375 MPa and 592 MPa, respectively.

The modal properties of the bridge column identified through eigenvalue analysis evidence that the response is essentially governed by the 1st mode (T_1 = 0.78 s). Nevertheless, the concrete block on the column introduces a significant rotational inertia that governs the second mode of vibration (T_2 = 0.14 s) and partially affects the fundamental mode (the effective modal mass equals 84% and 15% for the first and second mode, respectively). Analysis results indicate that despite the sectional response being a hardening one, the global pushover curve shows a noteworthy softening behaviour, reflecting the importance of second-order effects. Additional details regarding the test experimental protocol can be found in Carrea (2010).

The second group of structures considered in this study are two RC 3D frames subjected to four motions of increasing intensity applied simultaneously in the two horizontal directions. They were tested at *LNEC-3D* shaking table under the initiative of the "Blind Test Challenge", included in the 15th World Conference on Earthquake Engineering (Costa et al., 2012). The two structures are geometrically identical (Fig.3 (right)), but have different reinforcement details. Structure 2 was conceived without capacity design considerations, resulting in a strong beam/weak column mechanism. On the other hand, the reinforcement of Structure 3 was designed in order to develop a ductile response. The measured concrete compressive strength ranged from 30 MPa to 36 MPa. Regarding the reinforcement steel, the yield strength was of 560 MPa, 559 MPa and 566 MPa, respectively for rebar diameters of ∅8, ∅10 and ∅12. The ultimate strain of the longitudinal rebars varies between 628 MPa and 654 MPa. The behaviour of the two structures is essentially governed by the two first modes of vibration defined in the two main directions (T_1 = 0.31 s in X and T_2 = 0.28 s in Y). A fourth mode of vibration (T_4 = 0.15 s), reflecting a rotation around the vertical axis, contributes significantly to the torsional response of the structure. When subjected to a static lateral load, the two structures exhibit a softening response both at global and sectional levels.

Sensitivity Parameters

The following Table.2 summarises the sensitivity parameters and associated properties considered in the present study. The text in bold identifies the properties of the reference model that represent, based on the current state-of-the-art, customary options. They were preserved constant when performing the analyses on the additional parameters. The EVD properties, on the other hand, were defined in an

Table 2. Sensitivity parameters considered in the parametric study

Sensitivity parameters	Properties	
Damping model	No Damping	
	TSPD ISPD MPD	0.5% 1% 1.5% 2% 5%
Element discretization scheme	10 IPs	
	End IP = 0.5 L_p	
	End IP = L_p	
Strain penetration	No SP	
	Longer element	
	Base Spring	

initial stage, and the solutions that produced the best results were used in the analysis of the remaining parameters. The numerical modelling was carried out using SeismoStruct (Seismosoft, 2013).

Goodness-of-fit Evaluation

The goodness-of-fit of the different sensitivity analyses requires the identification of both structural response parameters as well as a methodology to efficiently process the data obtained from experimental and numerical analysis. Lateral displacements and accelerations were chosen since they are internationally accepted indicators of the structural response at the global level and are usually made available after experimental campaigns.

In order to assess the effectiveness of each modelling assumption with respect to the experimental results, two distinct relative error measures were used. The first one, named Frequency Domain Error (FDE) index, is based on the characteristics of the frequencies contained in the signals under analysis (Dragovich and Lepage, 2009). Considering the Fourier Transform of both the measured and simulated signals, this method quantifies the error associated with both amplitude and phase differences between the two signals (Fig.4). It equals 0 for a perfect correlation and 1 when the two signals are 180° out-of-phase (Lepage et al., 2008).

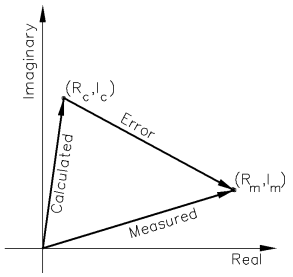

$$FDE = \frac{\sum_{i=f1}^{f2}\sqrt{(R_{Mi}-R_{Ci})^2+(I_{Mi}-I_{Ci})^2}}{\sum_{i=f1}^{f2}\sqrt{(R_{Mi}+I_{Mi})^2+(R_{Ci}+I_{Ci})^2}} \quad (5)$$

Figure 4. Graphical representation and FDE index equation (Dragovich and Lepage, 2009)

In Eq.5, R_{Mi} / I_{Mi} and R_{Ci} / I_{Ci} are the real and imaginary components of the measured and calculated signal, while f_1 and f_2 are the starting and ending frequencies adopted in the error measure. They are defined as functions of the fundamental period of the structures: respectively $1/(4T_1)$ and $1/(0.1T_1)$.

The second error measure represents a more conventional approach and consists in determining the relative error measured between the maximum response parameter (displacement or acceleration) obtained analytically and the benchmark experimental value, for each record separately:

$$Error_{Max.\ i,j} = \frac{max(Resp_{num,i,j}) - max(Resp_{exp,i,j})}{max(Resp_{exp,i,j})} \quad (6)$$

In the previous equation, the index ‘i' indicates each individual record among the full set, while the index ‘j’ represents the values measured in the positive and negative side of each direction. It is important to note that while the first measure returns positive relative error values, the second option yields either positive or negative relative error values. Moreover, values that approach 0 indicate good response correlations for both error measures considered. A summary flowchart reflecting the fundamental properties and main stages of the current parametric study is depicted in Fig.5:

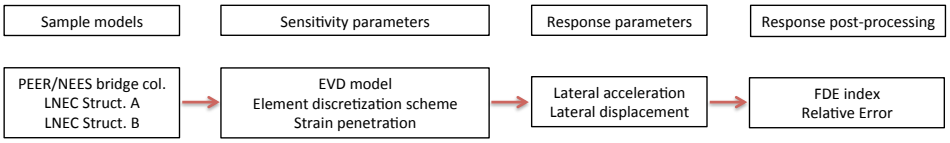

Figure 5. Outline of parametric study

STRUCTURAL RESPONSE

The present section shows the results of the sensitivity study carried out with nonlinear dynamic analyses. In the subsequent plots, the error computed at each individual record is illustrated with filled or empty markers, depending on the loading direction. In addition, the black circles with the associated error bars represent the mean value and the standard deviation of the error computed for the complete set of records. Due to space limitations, and given that the following plots follow essentially the same format, the legend is presented only at the first figure. The "+" and "-" symbols are used to distinguish the relative error associated with both signs for each direction. For the FDE index case, such distinction is not applicable and the symbol corresponding to the positive sign is used to identify the different records.

Equivalent Viscous Damping

The following paragraphs discuss the comparisons between the experimental data and the results obtained for the three structures assuming different EVD properties. Fig.6 presents the evolution of the FDE index. The errors computed for the displacements indicate that the numerical model better simulates the experimental results for EVD models featuring low percentages of critical damping (roughly between 0.5% and 2%). For such range of values the damping forces are comparatively small and therefore it is not immediate to tell the differences between MPD or SPD models by looking at this response parameter. Yet, it is clear that as the percentage of critical damping increases, the error associated with the ISPD increases significantly with respect to the TSPD and MPD counterparts. On the other hand, the use of 0% damping produces a slight increase of the FDE error, associated with an overestimation of the displacements.

Fig.7 (left) presents the relative error associated with the measured accelerations in Structure 1. It is interesting to note that the averaged maximum accelerations are generally better estimated with MPD models, independently of the percentage of critical damping considered. This effect results partly from the overestimation of the accelerations during EQ4. In order to clarify the reasons of such peculiar behaviour, the central and right plots in the following figure show the variation of the transverse and rotational accelerations at the top of the pier considering both MPD and TSPD with 0.5% of critical damping.

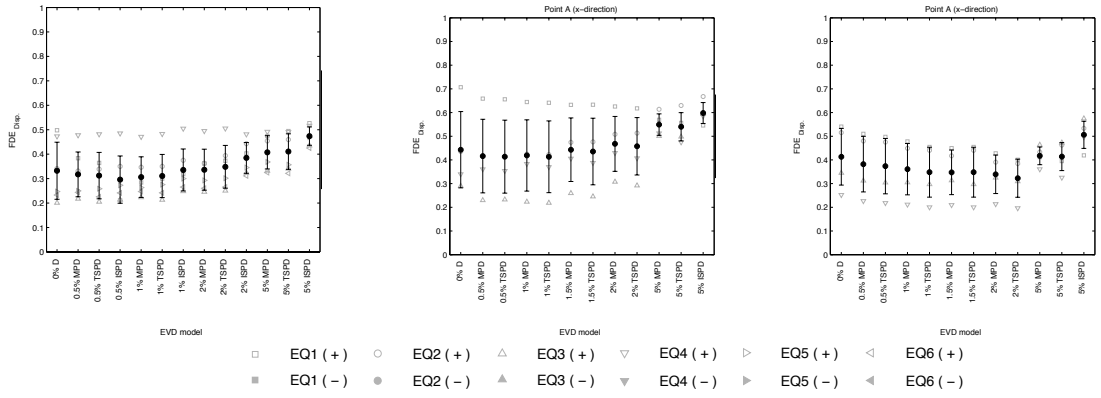

Figure 6. FDE associated with the displacements measured in Structure 1, 2, and 3 (respectively on the left, centre, and right side plots), considering different EVD models

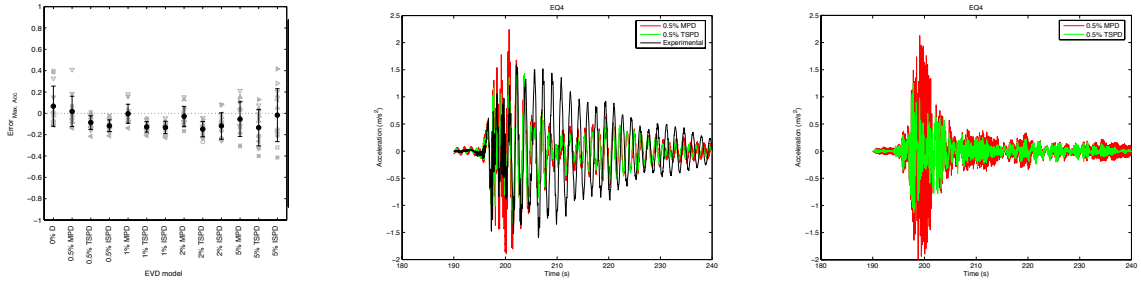

Figure 7. Error associated with the accelerations measured in Structure 1, considering different EVD models. From left to right: maximum error, transverse and rotational history of accelerations during EQ4

The central plot presented in the previous figure shows a significant difference in the transverse accelerations computed with both damping models around Time≈200s. After this point, both models produce similar values, somehow lower than the experimental ones. This localized effect seems to be associated with the way that SPD and MPD models deal with the contribution of higher-mode effects (second mode, in this case). In the right side plot, the high-frequency rotational accelerations—response parameter associated with the second mode of vibration—exhibit also a larger difference around Time≈200s. In this case the values computed with MPD are about four times larger than the ones obtained with the TSPD model. Contrarily to this latter model, where the damping forces are larger for higher modes, in the MPD case the higher modes tend to become more important as they are always less damped than the fundamental mode of vibration.

Element Discretization

In the following, the response of the structures with the discretization options indicated in Table.1 is evaluated for the most accurate damping models identified in the previous section. The results presented in Fig.8 indicate that the lateral displacements in Structure 1 tend to increase with the number of IPs per element. Considering the hardening type of response at the section level, it would be expected that the response converged to an objective response for increased number of IPs. Yet, considering the small variability observed for both experimental displacements and accelerations, it is difficult to identify a discretization scheme that stands with respect to other. The results obtained for Structure 2 and 3 indicate that the use of a discretization scheme wherein the integration weight of the end IPs equal the expected plastic hinge length produces more accurate estimations of the global displacements. This observation is in line with the conclusions of previous studies, namely by Calabrese et al. (2010).

Despite the absence of reliable measurements of the base curvatures during the experimental tests, it is important to underline that this parameter is very sensitive to the adopted discretization. Fig.9 illustrates the variation of the base curvatures measured in Structure 1 during EQ1 and EQ3. As expected, while responding essentially in the linear range (EQ1), the simulated base curvatures are very similar. However, during large nonlinear excursions (EQ3), the base curvatures measured with 10 IPs reach values that are up to two times larger than the ones obtained with two elements with 3 IPs each. Considering the magnitude of the differences, and despite the absence of experimental validation, the results obtained point towards the need to implement regularization techniques in order to improve the simulation of the local response of the elements.

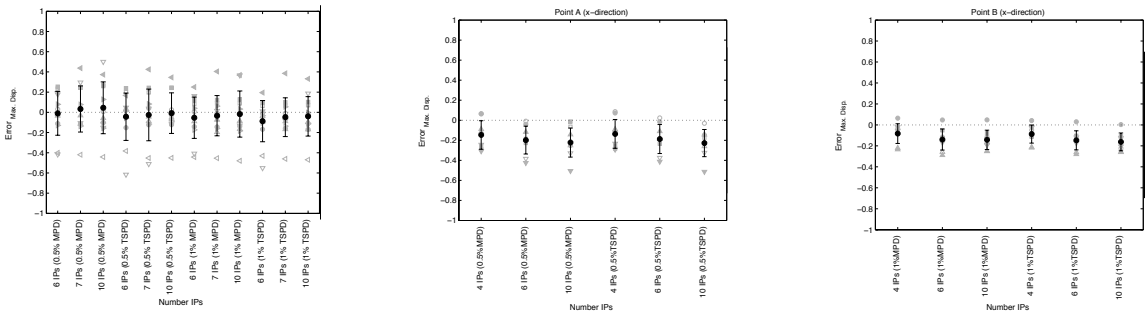

Figure 8. Errors associated with the maximum displacements measured in Structure 1, 2 and 3 (left to right), considering different number of IPs

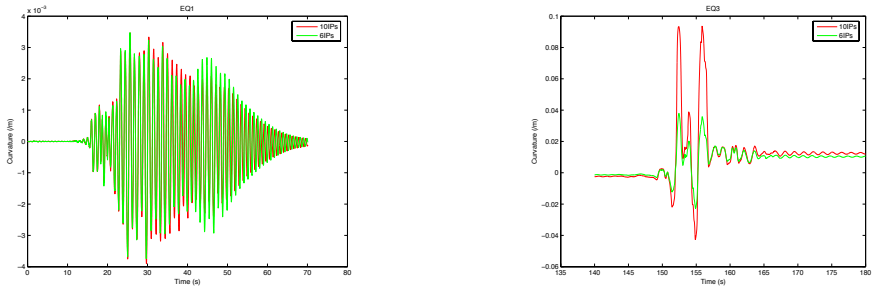

Figure 9. Variation of numerical curvatures on Structure 1 during EQ 1 (left) and EQ 3 (right)

Strain penetration

Despite recent developments with respect to the capability of implicitly accounting for the strain penetration (SP) effects at the element formulation level (briefly described previously), the options to model such localized nonlinear behaviour are still limited and insufficiently validated. Therefore, more conventional and simplified approaches as the use of a linear rotational spring or the elongation of the element were considered in the current work. The results are illustrated in Fig.10, indicating that both approaches improve the estimations with respect to the case where such "additional" flexibility is neglected. The use of a simple elongation of the element seems to provide more accurate displacements than the use of a rotational spring at the base of the columns. Such observation is also appreciable in the computed accelerations, although in that case the effects are less relevant. The results obtained for Structure 2 and Structure 3 follow a similar trend to the one presented before for Structure 1. However, it is important to highlight that the error computed for Structure 2 and 3 during EQ1 tend to be higher when considering the different SP models (Fig.11).

The previous observation results essentially from the behaviour of the structure when responding essentially in the elastic range. The displacement time-history depicted in Fig.12 indicates that the response is particularly different during EQ1, i.e. when the response of the structure is essentially elastic. This observation exposes an important limitation of current SP models that is associated with an (unrealistic) change in the modal properties of the structures. It is important to underline that both SP models are defined in order to replicate the joint flexibility upon yielding only. Hence, such approaches tend to overestimate the structural flexibility during elastic response.

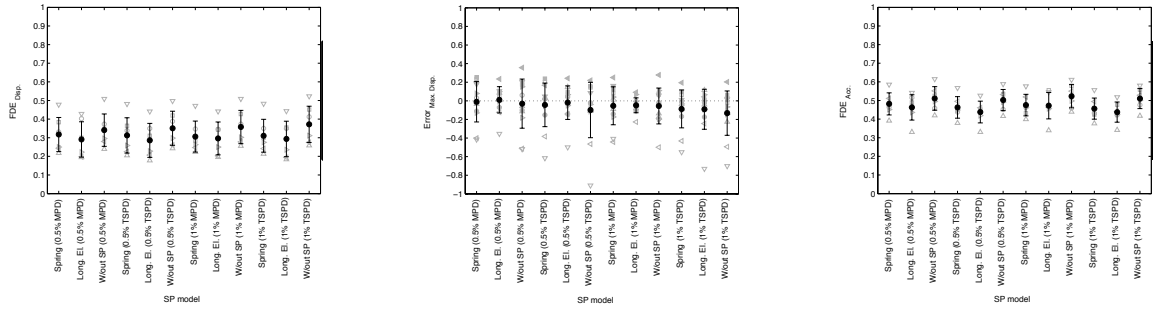

Figure 10. Errors measured in Structure 1 considering different strain penetration models

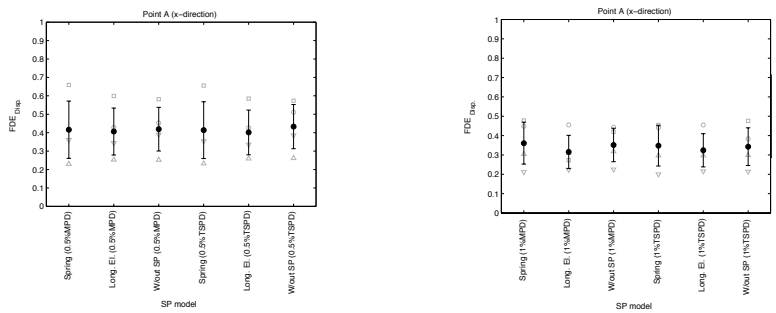

Figure 11. Errors associated with the displacements measured in Structure 2 (left) and 3 (right) considering different SP models

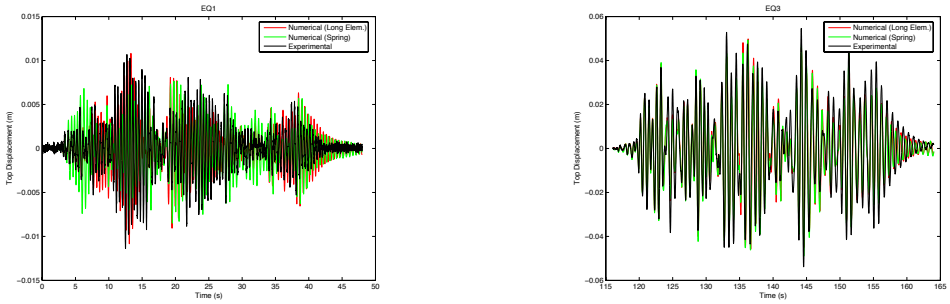

Figure 12. Displacements time-history measured during EQ 1 and 3 in Structure 2 (point A, direction X) for different SP models

CONCLUSIONS

Three RC structures tested experimentally in the recent past were numerically simulated considering alternative modelling options for distributed plasticity frame elements. The accuracy of each solution was appraised based on the comparison between the response parameters obtained numerically and those measured experimentally. The detailed analyses of two error measures yielded the following conclusions:

Most energy dissipation mechanisms in bare RC structures can be explicitly modelled by hysteretic material rules. Therefore, the use of equivalent damping models should be limited. Based on the analyses performed, enhanced performance was obtained with values of critical damping ranging from 0.5% to 2%. It was apparent that numerical analyses featuring larger levels of EVD tend to underestimate the structural response, whilst the use of no damping results in a slight overestimation of the response parameters. Considering the analysed response parameters and the abovementioned low values of damping, the study was unclear between the relative performance of mass-proportional damping and tangent-stiffness proportional damping.

The definition of a number of integration points per element such that the weighted length associated with the end IPs equals the expected plastic hinge length produces somewhat more accurate results. However, and despite the relatively small differences observed at the global level (i.e., regarding nodal displacements and accelerations), the curvatures computed at the ends of the elements are very sensitive to the adopted discretization. Further studies on the local response of RC finite elements are required.

Accounting for strain penetration effects can improve considerably the simulation of response parameters. Between the two selected modelling options, elongating the element by a strain penetration length appears to produce better results than the use of a rotational spring. Nonetheless, it should be highlighted that both approaches present various limitations. While both approaches change considerably the elastic properties of the structure (more significantly for the base spring approach), the use of a longer element results in a slight underestimation of the element forces.

REFERENCES

Almeida J P, Das S, Pinho R (2012) "Adaptive force-based frame element for regularized softening response," *Computers & Structures*, 102-103, 1–13

Bernal D. (1994) "Viscous Damping in Inelastic Structural Response," *Journal of Structural Engineering*, 120(4), 1240-1254

Calabrese A, Almeida J P, Pinho R (2010) "Numerical Issues in Distributed Inelasticity Modeling of RC Frame Elements for Seismic Analysis," *Journal of Earthquake Engineering*, 14(sup1), 38–68

Carrea F (2010) Shake-Table Test on a Full-Scale Bridge Reinforced Concrete Column, MSc Thesis, U. Bologna, Italy

Chopra A K (1995) Dynamic of Structures, Prentice Hall

Coleman J, Spacone E (2001), Localization Issues in Force-Based Frame Elements, *Journal of Structural Engineering*, 127(11), 1257–1265

Correia A A. (2011) A Pile-Head Macro-Element Approach to Seismic Design of Monoshaft-Supported Bridges, Ph.D. Thesis, ROSE School, IUSS Pavia, Italy

Correia A A, Almeida J, Pinho R (2013), Seismic Energy Dissipation in Inelastic Frames: Understanding State-of-the-Practice Damping Models, Structural Engineering International, 23(2), 148–158,.

Costa A, Campos Costa A, Candeias P, Guerreiro L, Mendes L (2012) "15WCEE Blind Test Challenge – Design Report," *Technical report*.

Dragovich J, Lepage A (2009) "FDE index for goodness-of-fit between measured and calculated response signals," *Earthquake Engineering & Structural Dynamics*, 38(15), 1751–1758

Girard C, Bastien J (2002) "Finite-Element Bond-Slip Model for Concrete Columns under Cyclic Loads," *Journal of Structural Engineering*, 128(12), 1502-1510

Hall J (2006) "Problems encountered from the use (or misuse) of Rayleigh damping," *Earthquake Engng Struct. Dyn.*, 35(5), 525–545, doi:10.1002/eqe.541.

Hines E, Restrepo J J, Seible F (2004) "Force-Displacement Characterization of Well-Confined Bridge Piers," *ACI Struc. Jour.*, no.101-S54, 537-548

Jehel P, Léger P, Ibrahimbegovic A (2013) "Initial versus tangent stiffness-based Rayleigh damping in inelastic time history seismic analyses," *Earthquake Engng Struct. Dyn.*, n/a–n/a

Jendele L, Cervenka J (2006) "Finite element modelling of reinforcement with bond," *Computers & Structures*, 84(28), 1780–1791

Lepage A, Delgado S, Dragovich J (2008) "Appropriate Models For Practical Nonlinear Dynamic Analysis of Reinforced Concrete Frames," *Proceedings of the 14th WCEE*, pp. 1–8

Monti G, Spacone E (2000) "Reinforced Concrete Fiber Beam Element With Bond-Slip," *Journal of Structural Engineering*, 126(6), 654–661

NEES@UCSD, (2010) "Concrete Column Blind Prediction Contest," Available from URL: http://nisee2.berkeley.edu/peer/prediction_contest

Priestley N, Grant D (2005) "Viscous Damping in Seismic Design and Analysis," *Journal of Earthquake Engineering*, 9(2), 229–255

Priestley N, Calvi G M, Kowalsky M J (2007), Displacement-Based Seismic Design of Structures, IUSS Press

Salem H, Maekawa K (2004) "Pre- and Postyield Finite Element Method Simulation of Bond of Ribbed Reinforcing Bars," *Journal of Structural Engineering*, 130(4), 671-680

Scott M, Fenves G (2006) "Plastic Hinge Integration Methods for Force-Based Beam-Column Elements," *J. Struct. Eng.* 132, 244–252

Scott M, Hamutçuoğlu O M (2008) "Numerically consistent regularization of force-based frame elements," *Int. J. Numer. Meth. Engng*, 76(10), 1612–1631

Seismosoft (2013). SeismoStruct - A computer program for static and dynamic nonlinear analysis of framed structures, available from URL: www.seismosoft.com

Sezen H, Moehle J (2004) "Strength and Deformation Capacity of Reinforced Concrete Columns with Limited Ductility," *Proceedings of the 13th WCEE*

Sousa R, Eroğlu T, Kazantzidou Firtinidou D, Kohrangi M, Sousa L, Nascimbene R, Pinho R (2012) "Effect of Different Modelling Assumptions on the Seismic Response of RC Structures," *Proceedings of the 15th WCEE*

Sritharan S, Priestley N, Seible F (2000) "Nonlinear finite element analyses of concrete bridge joint systems subjected to seismic actions," *Finite Elements in Analysis and Design*

Yazgan U, Dazio A (2011a) "Simulating Maximum and Residual Displacements of RC Structures: I. Accuracy," *Earthquake Spectra*, 27(4), 1187–1202

Yazgan U, Dazio A (2011b) "Simulating Maximum and Residual Displacements of RC Structures: II. Sensitivity," *Earthquake Spectra* 27(4), 1203–1218

Zhao J, Sritharan S (2007) "Modeling of Strain Penetration Effects in Fiber-Based Analysis of 2 Reinforced Concrete Structures," *ACI Struc. Jour*.